Heliyon 9 (2023) e20178

Contents lists available at ScienceDirect

Heliyon

journal homepage: www.cell.com/heliyon

Novel immune checkpoint-related gene model to predict prognosis and treatment responsiveness in low-grade gliomas

Yangyang Guo [a,1], Jingxia Bao [b,1], Danfeng Lin [b,1], Kai Hong [a], Kenan Cen [c], Jie Sun [a], Zhepei Wang [a,**], Zhixuan Wu [b,*]

[a] Department of Neurosurgery, The First Affiliated Hospital of Ningbo University, Haishu District, Ningbo, 315010, Zhejiang, People's Republic of China
[b] Department of Breast Surgery, First Affiliated Hospital of Wenzhou Medical University, Wenzhou, 325000, Zhejiang, People's Republic of China
[c] The Affiliated Hospital of Medical School of Ningbo University, Jiangbei District, Ningbo, 315020, Zhejiang, People's Republic of China

ARTICLE INFO

Keywords:
Low-grade gliomas
Immune checkpoints
Gene signature
Survival analysis
Therapeutic response

ABSTRACT

Recently, studies have shown that immune checkpoint-related genes (ICGs) are instrumental in maintaining immune homeostasis and can be regarded as potential therapeutic targets. However, the prognostic applications of ICGs require further elucidation in low-grade glioma (LGG) cases. In the present study, a unique prognostic gene signature in LGG has been identified and validated as well based on ICGs as a means of facilitating clinical decision-making. The RNA-seq data as well as corresponding clinical data of LGG samples have been retrieved utilizing the Cancer Genome Atlas (TCGA) and Gene Expression Omnibus (GEO) databases. ICG-defined non-negative matrix factorization (NMF) clustering was performed to categorize patients with LGG into two molecular subtypes with different prognoses, clinical traits, and immune microenvironments. In the TCGA database, a signature integrating 8 genes has been developed utilizing the LASSO Cox method and validated in the GEO database. The signature developed is superior to other well-recognized signatures in terms of predicting the survival probability of patients with LGG. This 8-gene signature was then subsequently applied to categorize patients into high- and low-risk groups, and differences between them in terms of gene alteration frequency were observed. There were remarkable variations in IDH1 (91% and 64%) across low-as well as high-risk groups. Additionally, various analyses like function enrichment, tumor immune microenvironment, and chemotherapy drug sensitivity revealed significant variations across high- and low-risk populations. Overall, this 8-gene signature may function as a useful tool for prognosis and immunotherapy outcome predictions among LGG patients.

1. Introduction

In children, gliomas are the most common primary solid tumor of the central nervous system, with a prevalence of around 6 per 100,000 [1]. Based on the World Health Organization's 2021 grading criteria, gliomas are classified into adult-type diffuse gliomas,

* Corresponding author.
** Corresponding author.
E-mail addresses: fagoce@126.com (Z. Wang), wuzhixuan0922@163.com (Z. Wu).
[1] Equal contribution and first authorship.

https://doi.org/10.1016/j.heliyon.2023.e20178
Received 3 April 2023; Received in revised form 5 September 2023; Accepted 13 September 2023
Available online 14 September 2023

pediatric-type diffuse low- and high-grade gliomas, and circumscribed astrocytic gliomas [2]. In addition, 20% of all glioma cases are low-grade gliomas (LGGs), characterized by extensive invasion and a low rate of proliferation [3]. Although LGGs are distinguished by their milder biological behavior and better response to treatment [4], it is imperative to remember that they are precancerous tumors and carry a potential risk of progressing to high-grade gliomas (HGGs) [5]. The standard of care for LGGs is surgical resection; however, this treatment option is fraught with complications due to small and residual tumors, the existence of remaining tissue, and the high risk of recurrence [6]. Although patients may require chemotherapy or radiotherapy as part of their treatment strategy, these methods are associated with several adverse effects including vascular injury and cognitive impairment [6]. Therefore, finding reliable biomarkers for LGG is an urgent issue for prognosis prediction or applications as possible therapeutic targets.

Over the last decade, immunotherapy has made dramatic strides in cancer treatment [7]. Tumors express immune checkpoint molecules to evade immune surveillance [8]. Treatments that involve blocking immune checkpoints can intercept this pathway [9], owing to which it is considered a promising strategy to achieve anticancer immunity. This strategy involves the use of antibodies generated against the cytotoxic T-lymphocyte-associated protein 4 (CTLA-4), the programmed death receptor 1 (PD-1), or the PD-1 ligand (PD-L1) [10]. Recently, immunotherapy has been considered a tremendous success in terms of treating patients with gliomas [11]. However, anti-PD-1/PD-L1 immune checkpoint therapies have not been widely utilized in LGG patients, partly owing to suboptimal response to immunotherapy [12]. As a result, it is crucial to identify accurate biomarkers for immunotherapy against LGG to stratify individuals who may benefit from immune checkpoint therapies.

Currently, signatures focusing on immune checkpoint features have shown excellent predictive performance for the head as well as neck squamous cell carcinoma and lung adenocarcinoma [13,14]. It has not been revealed, however, whether or not immune checkpoint-related genes (ICGs) have a significant predictive role among LGG patients. To better evaluate prognosis and provide individualized therapy for patients with LGG, this research set out to discover ICGs associated with patient prognosis and construct a model.

2. Materials and methods

2.1. Data resources and processing

RNA-seq data for LGG and relevant clinical datasheets were acquired utilizing the Cancer Genome Atlas (TCGA) Data Portal (https://portal.gdc.cancer.gov/) and 512 samples in total were included and considered for the training cohort. Additionally, 85 samples (GSE4412) being extracted from the Gene Expression Omnibus (GEO) database (https://www.ncbi.nlm.nih.gov/geo/) and 443 samples (CGGA_693) being extracted from the Chinese Glioma Genome Atlas (CGGA) database have been set as the verification cohort. The transcription profiles were downloaded from GSE4412 as fragments per million kilobases (FPKM) to eliminate batch effects. In total, 282 ICGs as presented in Supplementary Table S1 have been identified by retrieving crucial genes of PD-1/PD-L1 as well as CTLA-4 signaling pathways utilizing the Kyoto Encyclopedia of Genes and Genomes (KEGG) and Reactome pathway databases.

2.2. Nonnegative matrix factorization (NMF) consensus clustering

NMF has been applied to detect latent characteristics in gene expression patterns by decomposing the original matrix into two nonnegative matrices [15]. The NMF R package has been utilized to perform cluster analysis on 512 TCGA data, revealing a correlation between the expression of 282 immune checkpoint-related genes in LGG and clinical characteristics. The optimal number of clusters was determined based on the co-occurrence, dispersion, and silhouette coefficient. In addition, overall survival (OS) and progression-free survival (PFS) were compared across groups using an R package called "survival". Microenvironmental cell population (MCP) differences were also evaluated with the use of the R packages limma, ggpubr, and MCPcounter [16].

2.3. Developing and validating an LGG prognostic model based on ICGs

The first step was to perform a univariate Cox regression on the ICG data for identifying genes that showed considerable association with the prognosis where P-value <0.05 was considered the criterion for inclusion. The prognostic model has been constructed based on the training cohort. Eight genes are considerably linked to OS in LGG patients after a series of factors were filtered utilizing the least absolute shrinkage and selection operator (LASSO) analysis using the glmnet R package. Each LGG patient's risk score (RS) was derived using the following formula:

$RS = \sum Coefi \times Xi$ ("*Coefi*" stands for coefficient and "*Xi*" is the corresponding ICG expression). Bounded by the median risk rating, the patients with LGG were categorized into the following two groups: low- and high-risk cohorts. The Kaplan–Meier (K–M) survival curves and receiver operating characteristic (ROC) curves were generated to validate model feasibility. The same procedure was applied to the GEO validation cohort for validating the power of the model.

2.4. Development and assessment of the predictive nomogram

Independent prognostic factors were screened through the implementation of univariate and multivariate Cox regression algorithms. The rms R package was applied for developing a nomogram that incorporates the prognostic model as well as clinical features, such as the patient's gender, age and grade of LGG. A calibration curve has been generated to evaluate nomogram deviations. Finally, the ROC curve has been utilized to verify the accuracy of the nomogram.

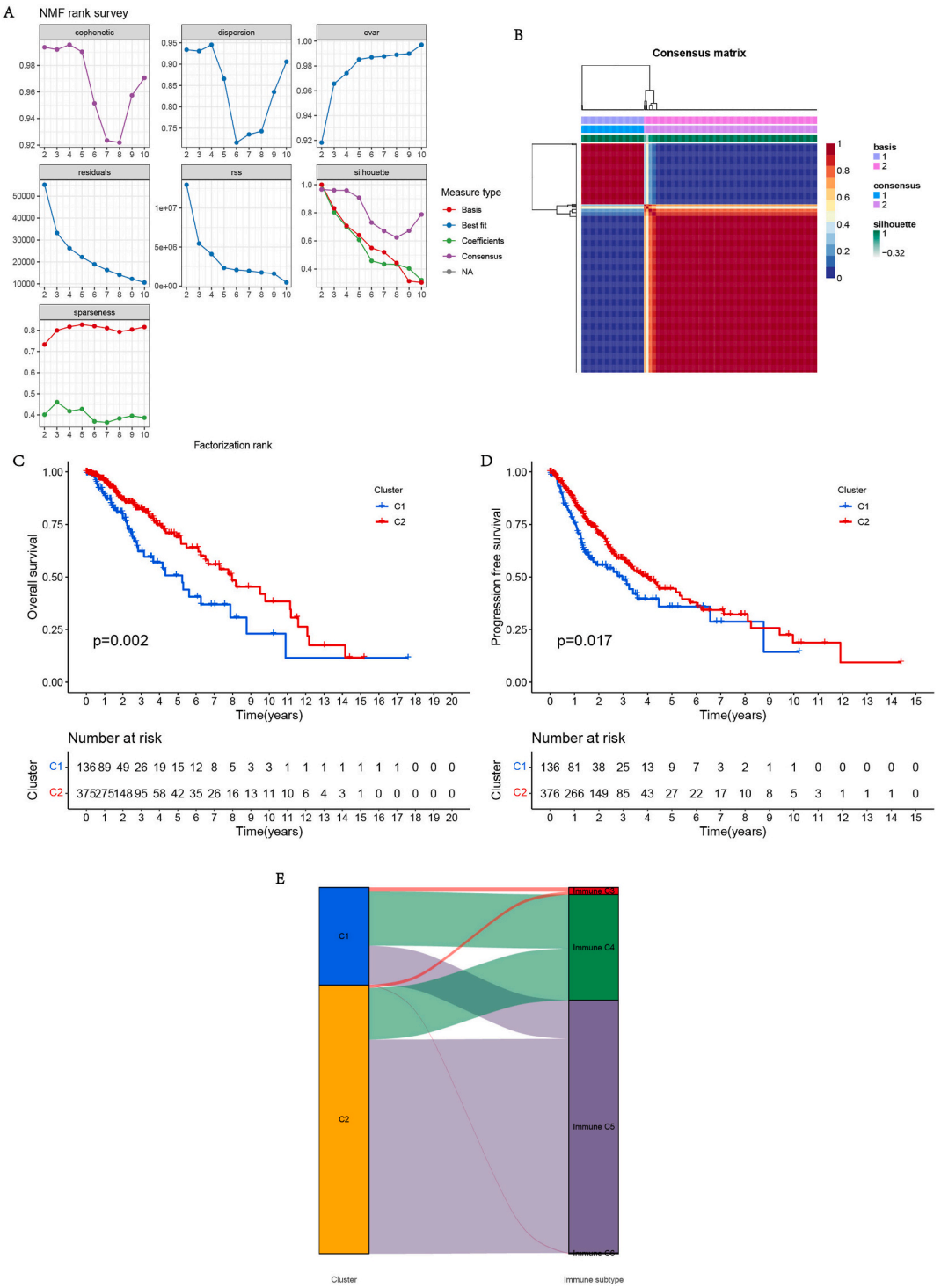

Fig. 1. Consensus clustering utilizing immune checkpoint-related genes: (A) Rank for 2–10 clusters based on factorization. (B) Gene expression heatmap for two clusters. (C, D) The K-M curve of OS ($p = 0.002$) and PFS ($p = 0.017$) in different clusters. (E) A Sankey diagram connecting NMF clusters and immune subtypes.

2.5. Tumor immune microenvironment and immunity analysis

Intergroup enrichment levels of cellular components or cellular immune responses based on the immune checkpoint-related signature were quantified using ESTIMATE [16], CIBESORT [17], QUANTISEQ [18], and TIMER [19]. Through a bubble plot, variations in immune responses under the algorithms were revealed. The intergroup comparisons of the immune checkpoint expression levels were performed utilizing packages like R, ggplot2, and reshape2.

2.6. Gene set enrichment analysis (GSEA) and functional enrichment analysis (FEA)

Gene ontology (GO) and KEGG analyses were conducted to assess the functions of differentially expressed genes between different risk groups determined utilizing the limma R package. The GSEA was performed between different risk subsets and the top 5 pathways were graphed [20]. Additionally, ssGSEA was performed and the enriched pathways for different risk groups were visualized using a heatmap.

2.7. Prediction of drug sensitivity based on the prognostic model

The Genomics of Cancer Drug Sensitivity database has been applied to make predictions about the sensitivity of patients with LGG to various chemotherapy drugs. The IC50 values (half of the maximum inhibition concentration) for 5-fluorouracil, AKT inhibitor VIII, bleomycin, crizotinib, dasatinib, gemcitabine, rapamycin, roscovitine, and salubrinal were calculated via pRRophetic algorithm with ridge regression. The results were visualized utilizing boxplots created with the R packages pRRophetic and ggplot2.

2.8. Mutation status analysis

The maftools R package has been applied to process somatic mutation profiles, whereas waterfall plots were generated to display genes with the highest mutation frequency.

2.9. Validation of the genes involved in the risk model

The HMO6 and U251 were cultured in DMEM and the U87 were cultured in MEM. All medium were supplemented with 10% fetal bovine serum (FBS) and 1% Penicillin/Streptomycin. Total RNA was isolated by TRIzol reagent (TaKaRa, Dalian, China). RNA integrity was detected by an Agilent 2100 bioanalyzer and the RNAs were sequenced on an Illumina platform.

2.10. Cell viability and colony formation assay

The sequence of MCC SiRNAs were shown in Supplementary Table S3. The SiRNAs were transiently transfected into U87 and U251 glioma cells. For cell viability experiments, cells were seeded onto 96-well plates at a density of 2000 cells/well. Subsequently, 10 μL CCK-8 was introduced into all wells. After 30 min, the absorbance was recorded at 450 nm. For colony formation assay, glioma cells were seeded in 6-well plates at a density of 1000/well. When approximately 100 cells were observed in a clonal cluster, glioma cells were fixed with 4% paraformaldehyde and then stained with crystal violet for 15 min.

2.11. Statistical analysis

All statistical analyses and visualizations were performed using the R software. The Spearman correlation analysis has been applied for assessing the association between the two continuous variables. Chi-square or Fisher's tests were utilized to examine categorical data, whereas Wilcoxon's test was applied for analyzing continuous variables. The p-values ($P < 0.05$) indicated statistical significance.

3. Results

3.1. NMF clustering analysis

The NMF algorithm was applied to cluster LGG cases in the total TCGA cohort based on the ICG expression, survival time, and survival status (Fig. 1A). Notably, the optimum number of clusters was found to be 2 (Fig. 1B). In order to have a clearer comprehension of the link between the two subtypes and prognosis, OS and PFS values have been subjected to comparison across the two clusters. The results indicated a poorer prognosis associated with cluster 1 in comparison to cluster 2 (Fig. 1C and D).

3.2. Comparison of clinical phenotypes, immune subtypes, and immune cell infiltration between molecular subtypes

A total of 33 cancers had been classified into the following six immune subtypes: C1 (wound healing), C2 (IFN-γdominant), C3 (inflammation), C4 (lymphocyte depletion), C5 (immune silencing), and C6 (TGF-β dominant) in a previous study [21]. Therefore, a Sankey diagram was generated to connect NMF clusters and immune subtypes (Fig. 1E). The plot showed that the C1 cluster was

connected with immune C3, C4, and C5; of these, immune C4 was the leading one. Furthermore, the C2 cluster included immune C3, C4, C5, and C6, in which immune C5 was the bulk. Additionally, immune cells levels were evaluated between two clusters via the MCPcounter R package. Fig. 2 showed that the C1 cluster had high infiltration of these cells in the immune microenvironment, except for neutrophils.

3.3. Mutation landscape of immune checkpoint-related genes

The cBio-Portal database was utilized to investigate the pertinent genetic mutations as illustrated in Fig. 3A. A total of 523 LGG tumor samples were analyzed and the gene alteration frequency of these ICGs was 15.68%. Regarding the gene mutation frequency, EGFR (6%) and PTEN (5%) were the most strikingly altered genes and showed missense mutations. In addition, missense mutations accounted for the vast majority of all mutation types in LCC patients. To get a deeper understanding of the correlations among these genes, a spearman correlation analysis has been conducted as illustrated in Fig. 3B. As per the results, EGFR, as well as PTEN, were found to possess a significantly high correlation ($P < 0.01$).

3.4. Development and verification of a prognostic gene model

In the training set (TCGA-LGG cohort), the univariate cox regression analysis has been performed to analyze the prognostic value of

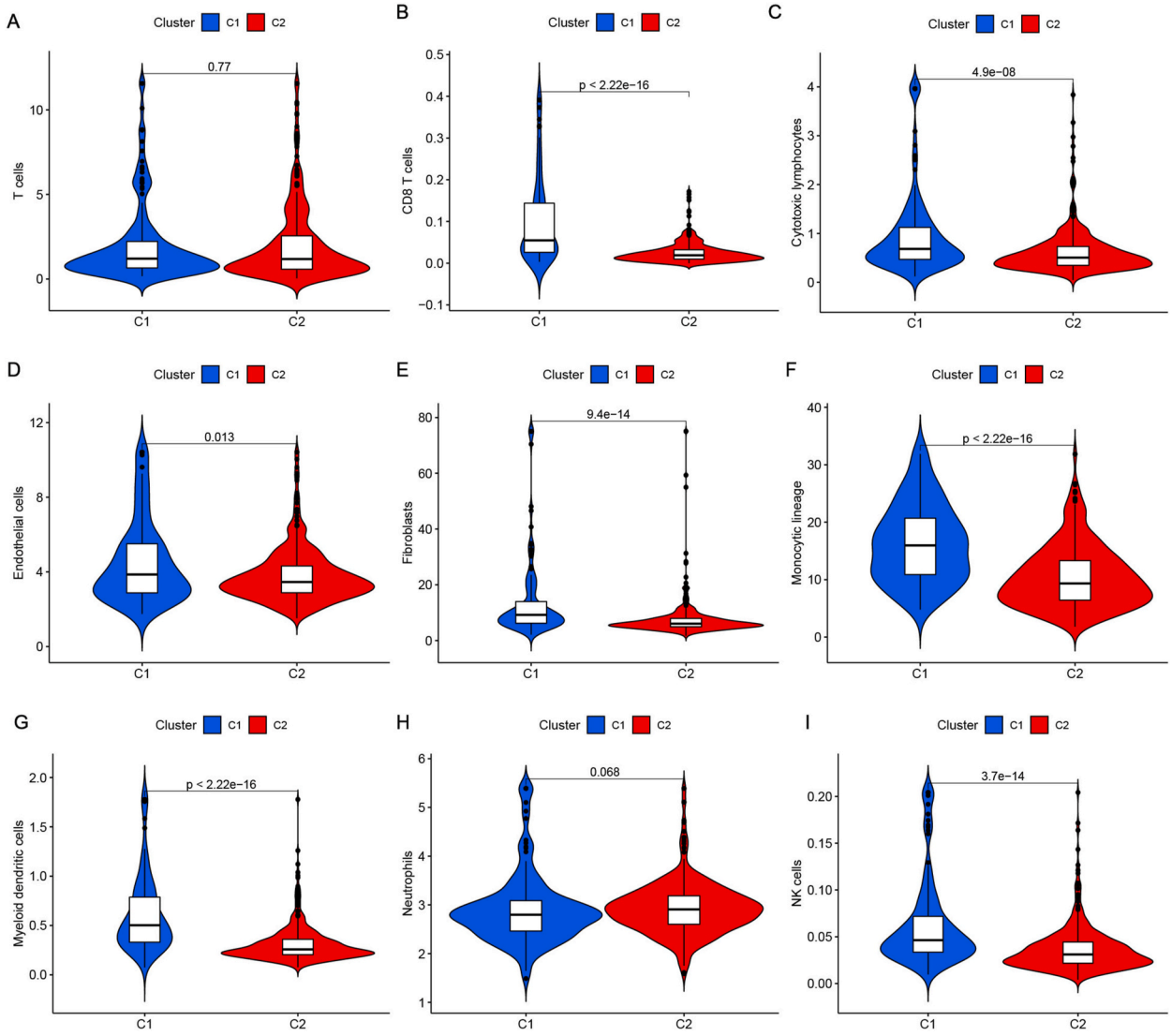

Fig. 2. Analysis of infiltrating immune cells and stromal cells including (A) T cells, (B) CD8T cells, (C) Cytotoxic lymphocytes, (D) Endothelial cells, (E) Fibroblasts, (F) Monocytic lineage, (G) Myeloid dendritic cells, (H) Neutrophils and (I) NK cells between the two clusters.

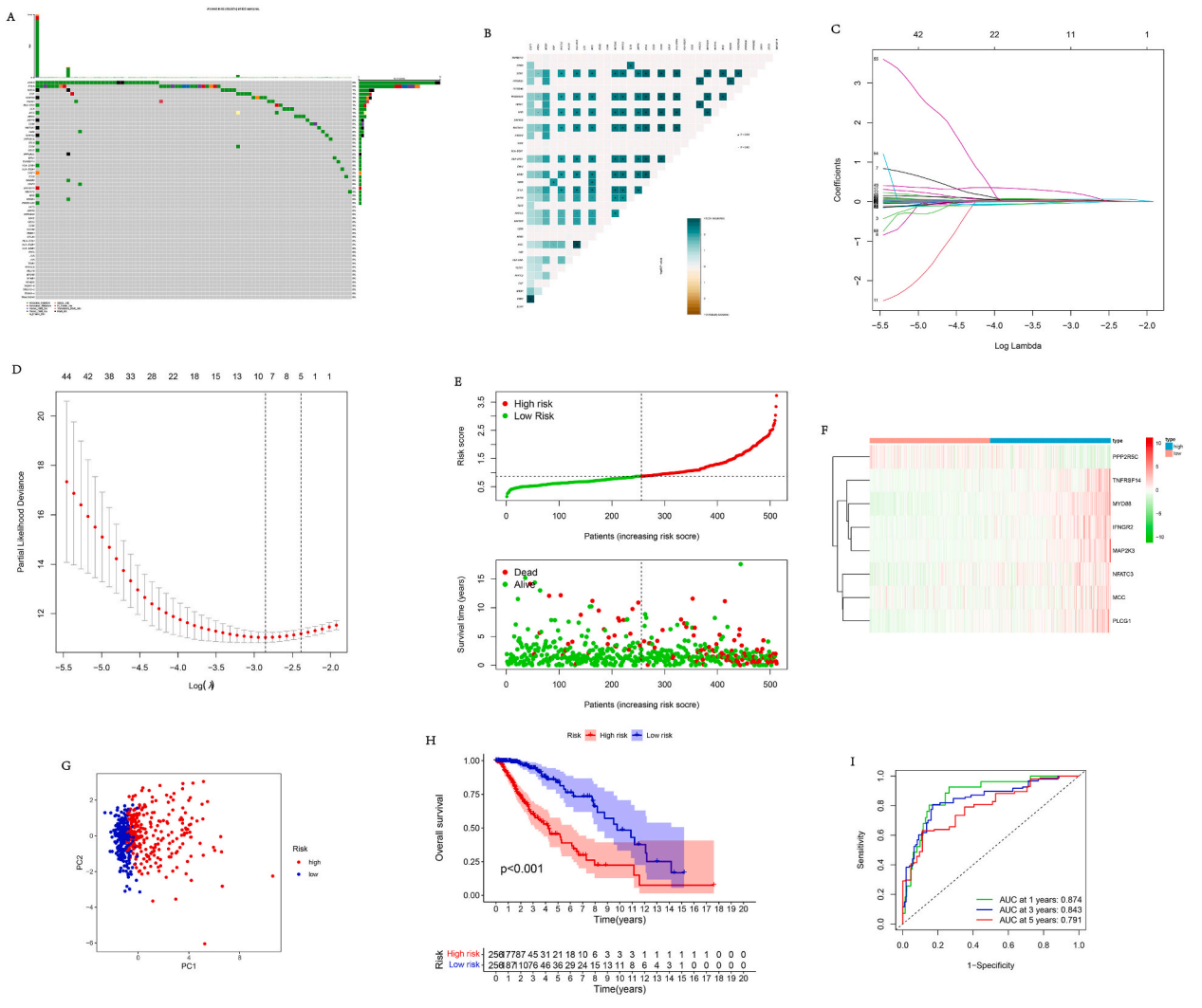

Fig. 3. (A) The gene mutation waterfall plot of 523 LGG tumor samples. (B) Spearman correlation analysis of major mutant genes. (C, D) LASSO regression analysis screened 8 prognostic related genes. (E) Patients' risk scores as well as survival status in the TCGA cohort. (F) A heatmap of the expression of 8 immune checkpoint-related genes in different risk groups. (G) The Principal Component Analysis (PCA) for the two risk groups. (H) Comparing OS across varied risk groups by K-M curves. (I) The 1-, 3-, and 5-year ROC curves of patients in the TCGA cohort.

all ICGs, which resulted in the identification of 58 prognostic-linked genes (Supplementary Table S2). Then, the LASSO Cox regression model has been utilized for the construction of a risk model. Finally, eight genes in total have been integrated as per the optimal λ value (Fig. 3C and D). The risk score has been derived as follows:

$$\text{risk score} = -0.028 \times \text{PPP2R5C(exp)} + 0.054 \times \text{TNFRSF14(exp)} + 0.005 \times \text{IFNGR2(exp)} + 0.037 \times \text{MAP2K3(exp)} + 0.003 \times \text{MCC(exp)} + 0.060 \times \text{MYD88(exp)} + 0.182 \times \text{NFATC3(exp)} + 0.023 \times \text{PLCG1(exp)}.$$

Based on the median risk score, LGG patients have been classified into high- and low-risk groups (Fig. 3E). Low-risk patients possess higher survival rates and longer survival times than patients in the high-risk training cohort. Moreover, when combined with the outcomes of the heatmap, these 8 genes' expression levels considerably varied across the two risk subgroups. In the high-risk group, PPP2R5C had low expression while others had a high expression, which is contrary to the low-risk group (Fig. 3F). Furthermore, the principal component analysis is revealing that patients with varied risks experienced a tendency to separate in two directions (Fig. 3G). The K-M curve revealed remarkably lowered survival probability and shorter OS in the high-risk group ($P < 0.001$, Fig. 3H). Assessment of the time-dependent ROC analysis revealed that the risk scores had high predictive accuracy. The areas under the ROC curve (AUC) were 0.874 for 1 year, 0.843 for 3 years, and 0.791 for 5 years (Fig. 3I).

Prognostic model robustness was validated via the same coefficients as the training cohort in the validation cohort and similar results were observed (Fig. 4, Supplementary Fig. 1).

3.5. Developing a nomogram

A Univariate Cox regression analysis of OS based on the TCGA cohort demonstrated various clinical features including age, grade, and risk score which all were found as potential prognostic indicators for LGG patients (Fig. 5A). In addition, the risk score proved as an independent prognostic predictor for LGG patients, as per the multivariate Cox regression analysis ($P < 0.001$, Fig. 5B). The nomogram, which takes into account several risk factors, can accurately predict a patient's prognosis. Improvement of the predictive performance was performed by integrating the clinical features and risk scores into the nomogram (Fig. 5C). Based on the nomogram model, every patient was assigned a total score that predicted 1-, 3-, and 5-year OS. The calibration curves showed that the nomogram had excellent performance in predicting 1-, 3-, and 5-year OS, which was similar to the actual OS (Fig. 5D). Additionally, the nomogram had AUC values of 0.893, 0.870, and 0.819 in the prediction of 1-, 3-, and 5-year survival rates, respectively, indicating that the nomogram may improve the OS prediction in comparison to traditional prognostic markers. (Fig. 5E–G).

3.6. Assessment of clinical phenotypes by risk score and prognostic analysis

A total of 253 (high-risk) and 247 (low-risk) samples have been analyzed and, gene alteration frequencies of 93.68% and 98.38% were recorded, respectively (Fig. 6A). Regarding the gene mutation frequency, Low-risk individuals had a remarkably greater frequency of altered genes such as IDH1 (91%) and TP53 (45%) compared to high-risk individuals (IDH1: 64% and TP53: 47%). The

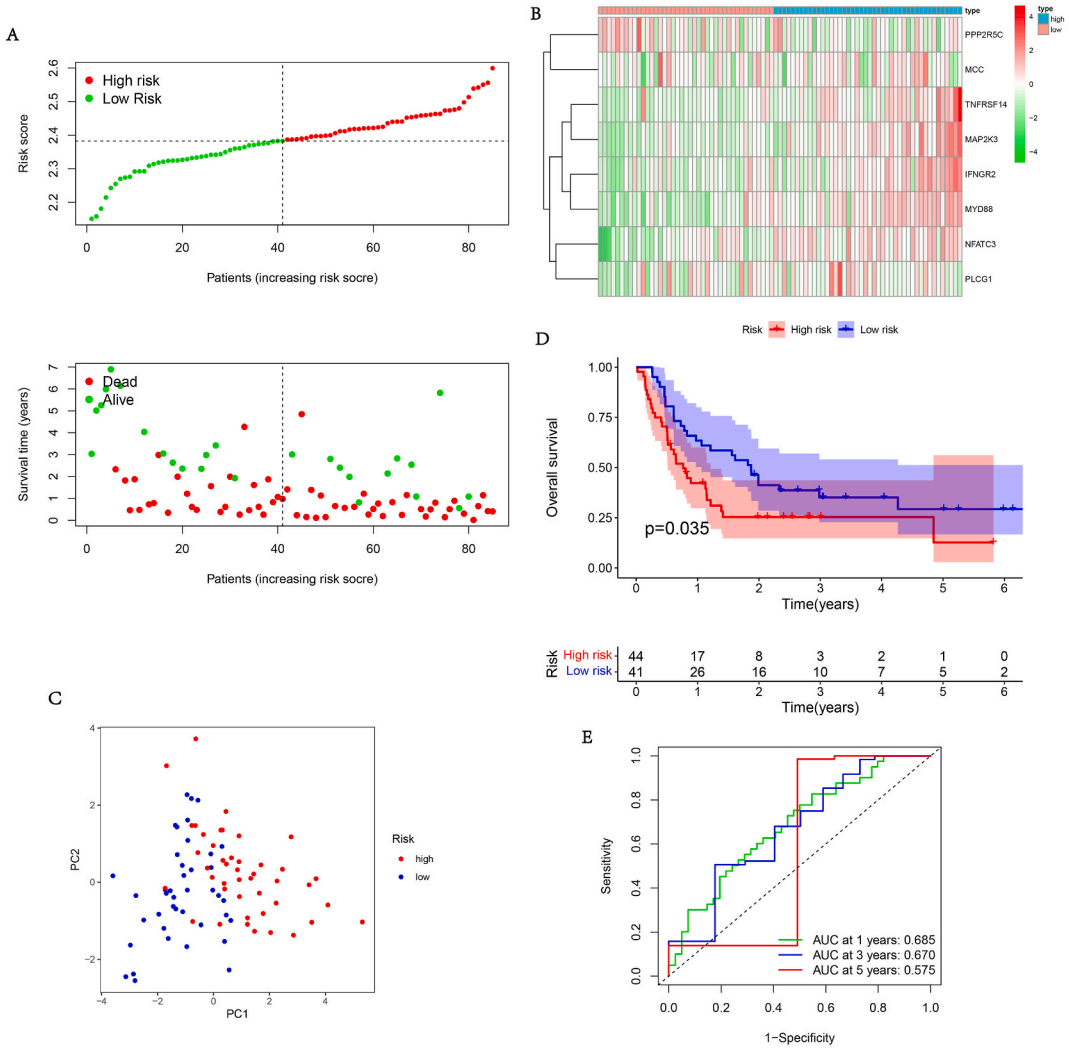

Fig. 4. The GSE4412 validation cohort confirms the performance of the eight-gene prognostic model. (A) The distribution of LGG patients' survival status as well as risk scores in the verification cohort. (B) A heatmap visualization of the expression of 8 genes involved in the model in the validation cohort. (C) PCA analysis of the two risk groups. (D) Survival curves for different risk groups in the validation set. (E) ROC curve and AUC demonstrating survival predicted by the prognostic model.

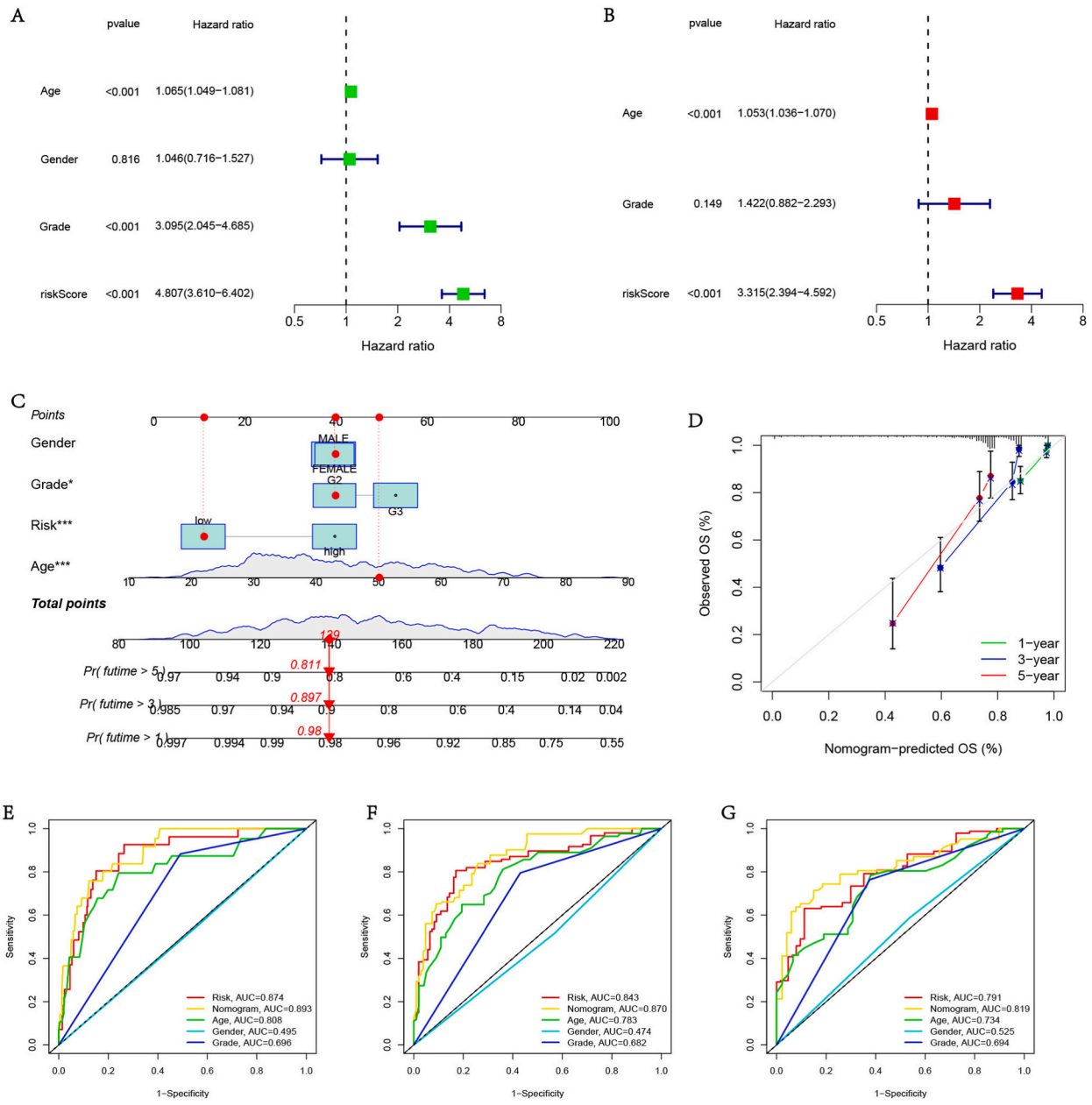

Fig. 5. Independence detection of the prognostic model and development of a predictive nomogram. (A, B) COX regression analysis for identifying independent prognostic variables. (C) Nomogram-predicted model for LGG. (D) Calibrations curves for predicting 1-, 3-, and 5-year OS. (E, F, G) ROC curves for the nomogram, clinical features, and risk scores.

missense mutation was the most prevalent type of mutation in both high-as well as low-risk groups. For establishing the clinical applicability of the prognostic model, the correlation of risk scores with clinicopathological features was investigated. Fig. 6B shows that age showed a significant correlation with the risk score. Moreover, subgroup survival analysis of the entire TCGA cohort has been conducted and its outcomes demonstrated that in the age >65 years, age ≤65 years, female, and male subgroups, patients in the high-risk group possess a poorer prognosis than those in the low-risk group (Fig. 6C–F).

3.7. Assessment of tumor immune microenvironment

The indicative role of prognostic models on the tumor immune microenvironment (TIME) was demonstrated by assessing immune scores, cells, and checkpoint expression levels in different risk groups. As anticipated, the high-risk group had higher values than the low-risk group in terms of the ESTIMATE, stroma, and immune scores (Fig. 7A). Next, a bubble and radar chart were generated to

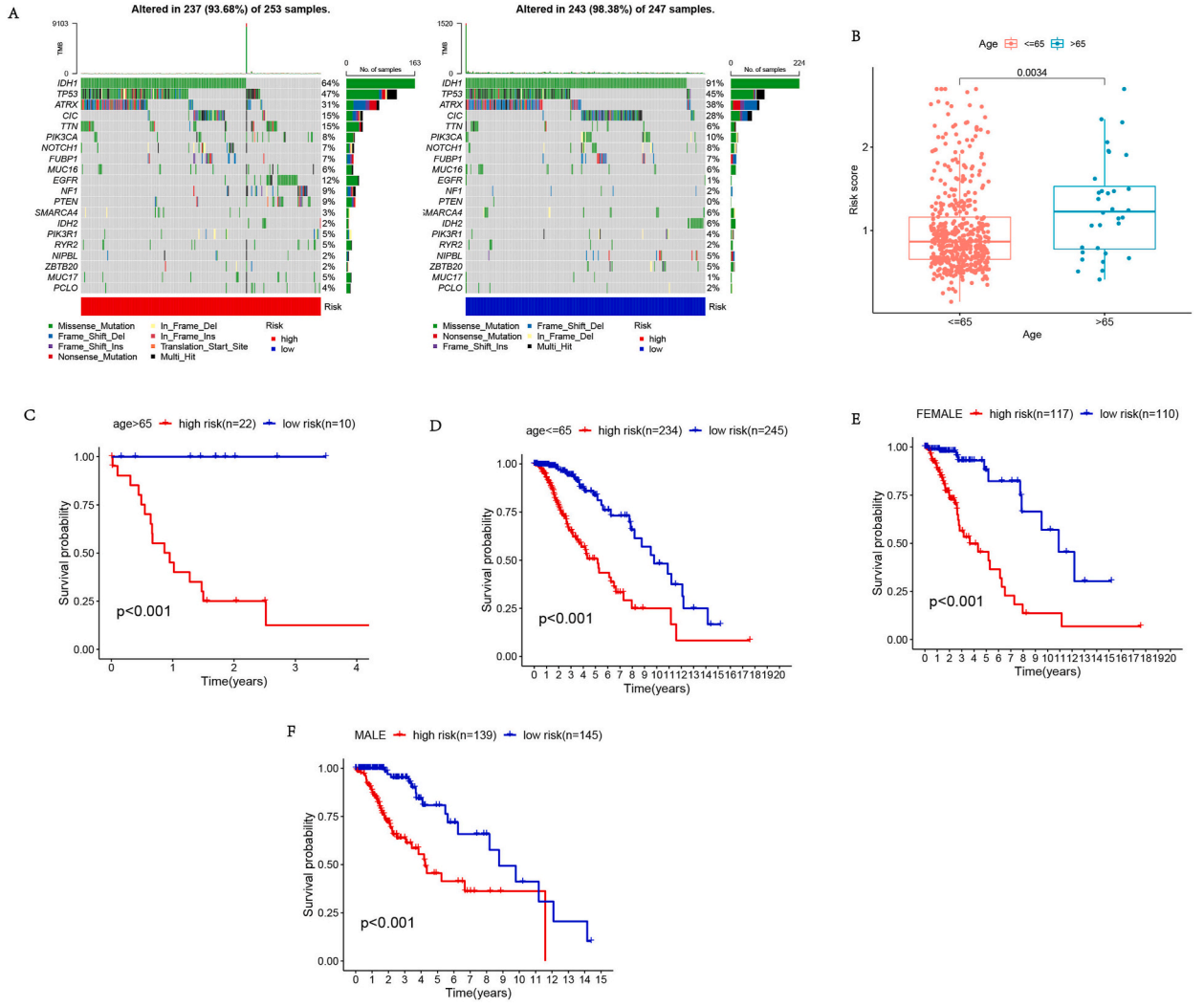

Fig. 6. Correlation analyses of the risk score and clinical phenotypes. (A) Gene mutation waterfall plot for high-risk and low-risk subgroups. (B) Comparison of the risk score between patients across varied age groups. (C–F) K-M curves showing subgroup analysis by age and gender.

demonstrate how the invasion of immune cells varies across the two risk groups (Fig. 7B and C). Moreover, as shown in Fig. 7D, eosinophils, monocytes, activated NK cells, and plasma cells had a negative correlation with the risk score, whereas macrophages (M0, M1, M2) as well as resting NK cells had a positive correlation with it. Considering the value of checkpoint inhibitor-based immunotherapy techniques, it has been evaluated how risk groups varied in the expression of immune-related genes (Fig. 8A–D). The vast majority of immune-related genes expression in the high-risk group was higher than that in the low-risk group. In addition, a correlation study was carried out to investigate the link between risk scores and TMB, and it was shown that risk scores had a positive correlation with TMB (Fig. 8E and F). The K–M curve integrating risk score and TMB had a favorable predictive performance for prognosis (Fig. 8G).

3.8. *Function enrichment analysis*

GSEA has been utilized for conducting GO and KEGG pathway analyses to further investigate the probable roles of ICGs in high- and low-risk groups. Fig. 9A–D demonstrate the top five important GO and KEGG-enriched pathways in two distinct risk categories. In addition, clustering analysis performed based on the enrichment scores of the relevant KEGG pathways revealed that limonene and pinene degradation, butanoate metabolism, propanoate metabolism, long-term potentiation, long-term depression, proximal tubule bicarbonate reclamation, cardiac muscle contraction, and pyruvate metabolism pathway all were substantially enriched in the low-risk group (Fig. 9E).

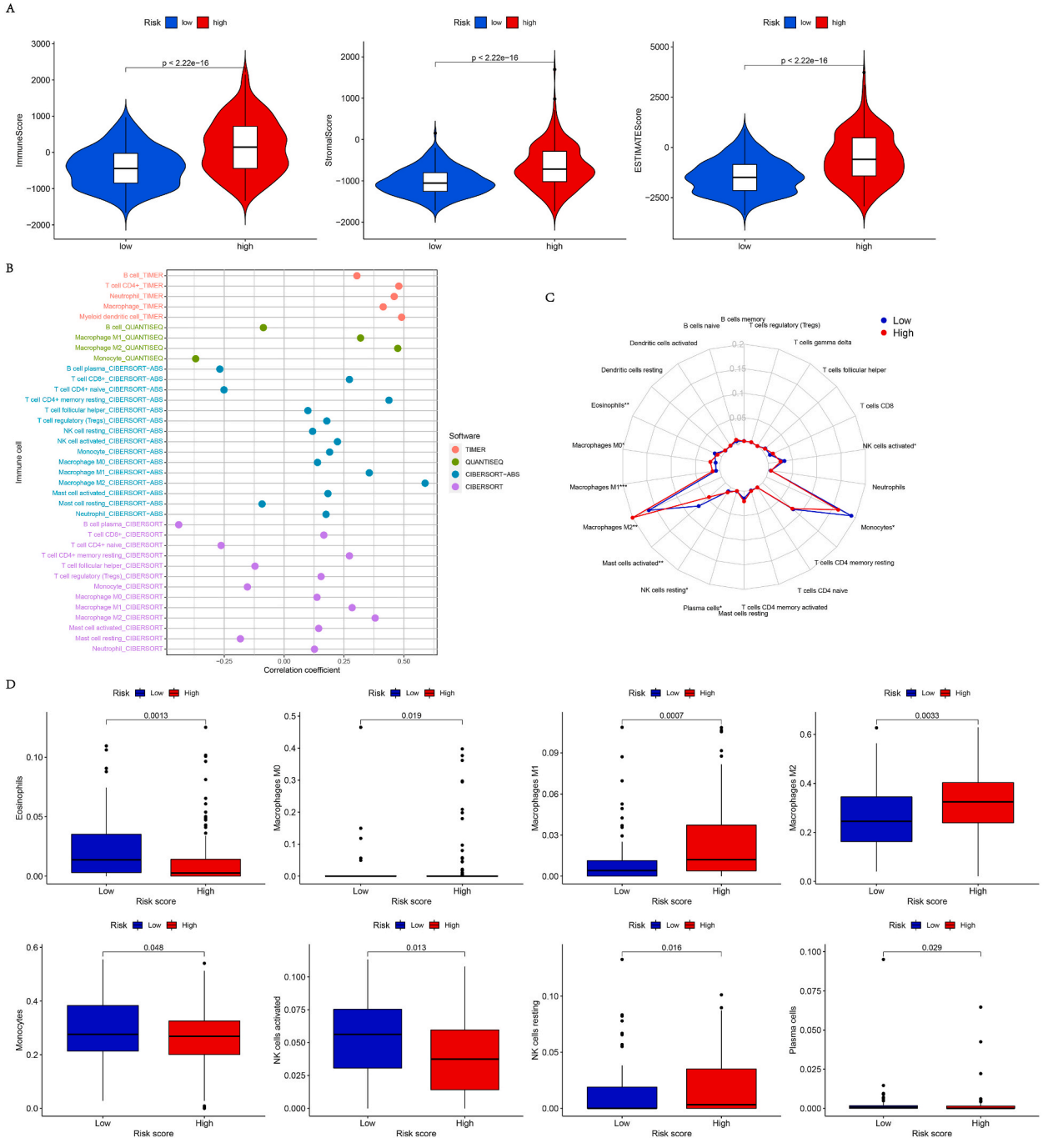

Fig. 7. Assessment of tumor immune microenvironment. (A) Comparisons of Immune Score, Stromal Score, and ESTIMATE Score in different risk groups. (B) A bubble chart of different immune cell infiltration algorithms. (C) A radar map of immune microenvironment cells across varied risk groups (D) Comparing immune cell infiltration across varied risk groups.

3.9. Chemotherapy drug sensitivity analysis

Chemotherapy is still one of the most prevalent treatment options for LGG. Therefore, the IC50 values of several chemotherapeutic agents in these two risk subgroups were further predicted by the pRRophetic algorithm. As shown in Fig. 10, higher predicted IC50s for two chemotherapy drugs (crizotinib and salubrinal) were observed in high-risk subgroups demonstrating beneficial effects to low-risk group patients from these drugs. Furthermore, patients in the high-risk groups showed a notably better response to 5-Fluorouracil, AKT inhibitor VIII, bleomycin, dasatinib, gemcitabine, rapamycin, and roscovitine.

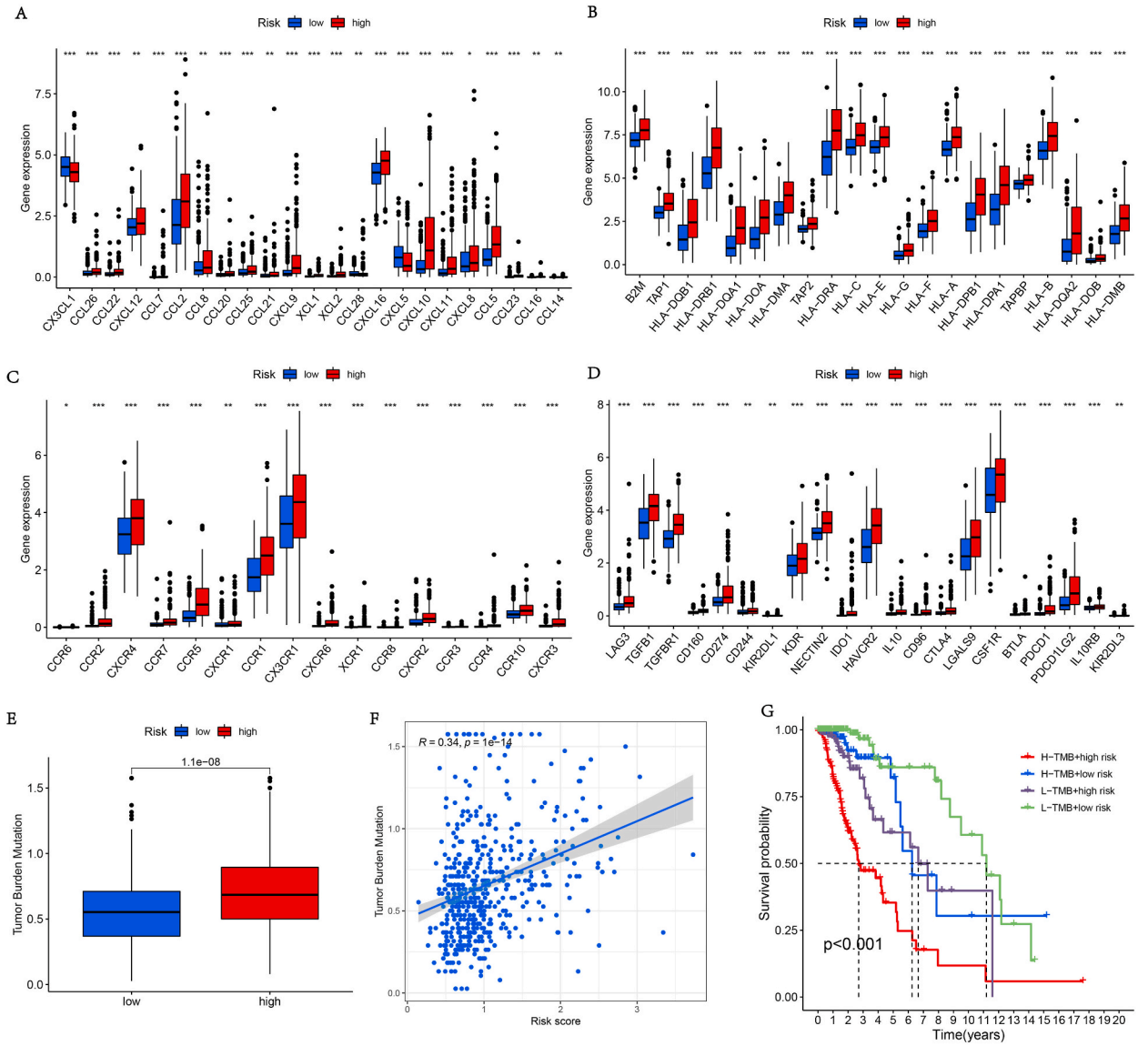

Fig. 8. (A–D) Boxplots representing immune checkpoints expression across varied risk groups. (E) Distribution of TMB across varied risk subgroups. (F) The correlation analysis of risk score with TMB. (G) K-M curves of TMB combined with the risk score.

3.10. Validation of the eight genes involved in the risk model

Next, we performed RNA-sequencing on the normal cell line HMO6 and tumor cell line U251 to further identify the expression levels of the eight genes involved in model construction. As shown in Fig. 11, MAP2K3, MCC, MYD88, NFATC3, PLCG1, TNFRSF14, IFNGR2 were remarkably up-regulated in the U251 cell line in comparison with the HMO6 cell line while PPP2R5C were down-regulated in the U251 cells. Therefore, eight genes were differentially expressed between tumor and normal cells, which may be biomarkers to predict the prognosis of LGG patients. In addition, the findings of CCK-8 and colony formation assays highlighted that MCC silencing inhibited cell proliferation in U87 and U251 cells (Fig. 12A–F).

4. Discussion

LGG has been identified as a universal primary malignant tumor of the central nervous system [22]. Although the current treatment strategy for LGG involves a combined administration of surgical resection, chemotherapy, and radiotherapy, which do improve clinical outcomes, still more than 50% of LGG patients progress to therapy-resistant high-grade aggressive glioma [23]. Owing to unclear pathogenesis and unsatisfied therapeutic effects, an in-depth analysis of the underlying mechanisms of LGG needs to be performed. Recent decades have seen significant advancements in the study of immune checkpoints, with multiple studies identifying key

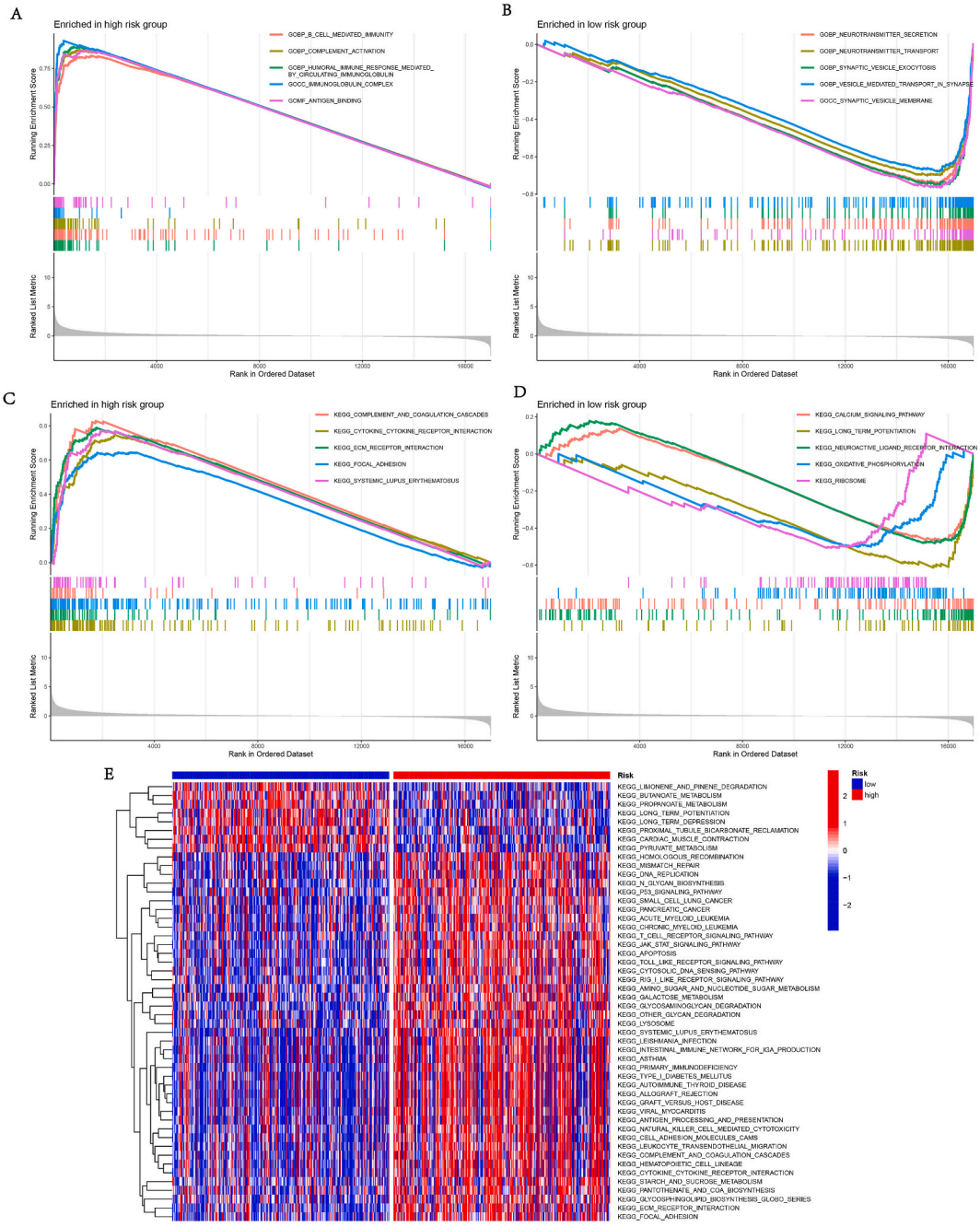

Fig. 9. Relationship between risk scores and pathways. (A–D) GSEA analysis in low- and high-risk LGG. (E) Heatmap of the ssGSEA scores of KEGG pathways in different risk groups.

molecules involved in the modulation of immune responses like certain immune checkpoint molecules (PD-1, PD-L1, CD28, Gal-9, and TIM-3) which are vital in the regulation of immune responses [24]. Nevertheless, cancer cells can escape surveillance and clearance from immune cells by excessively activating ICGs, which consequently accelerates tumor growth [25]. More research is needed to identify biomarkers and develop prognostic models based on ICGs that might aid in the prediction of survival in patients with LGG.

In the present study, first, LGG cases in the entire TCGA cohort were clustered according to the NMF algorithm based on 282 ICGs, and two molecular subtypes with significantly varied prognoses, clinical traits, as well as tumor immune microenvironment (TIME) were obtained. The C1 LGG group had a worse OS and PFS than the other group. A Sankey diagram showed that the C1 cluster was mainly connected with immune C4 (lymphocyte depletion), whereas the C2 cluster was linked to immune C5 (immune silencing). Notably, the C1 cluster showed a high infiltration of immune cells including monocytes, the precursors of tumor-associated

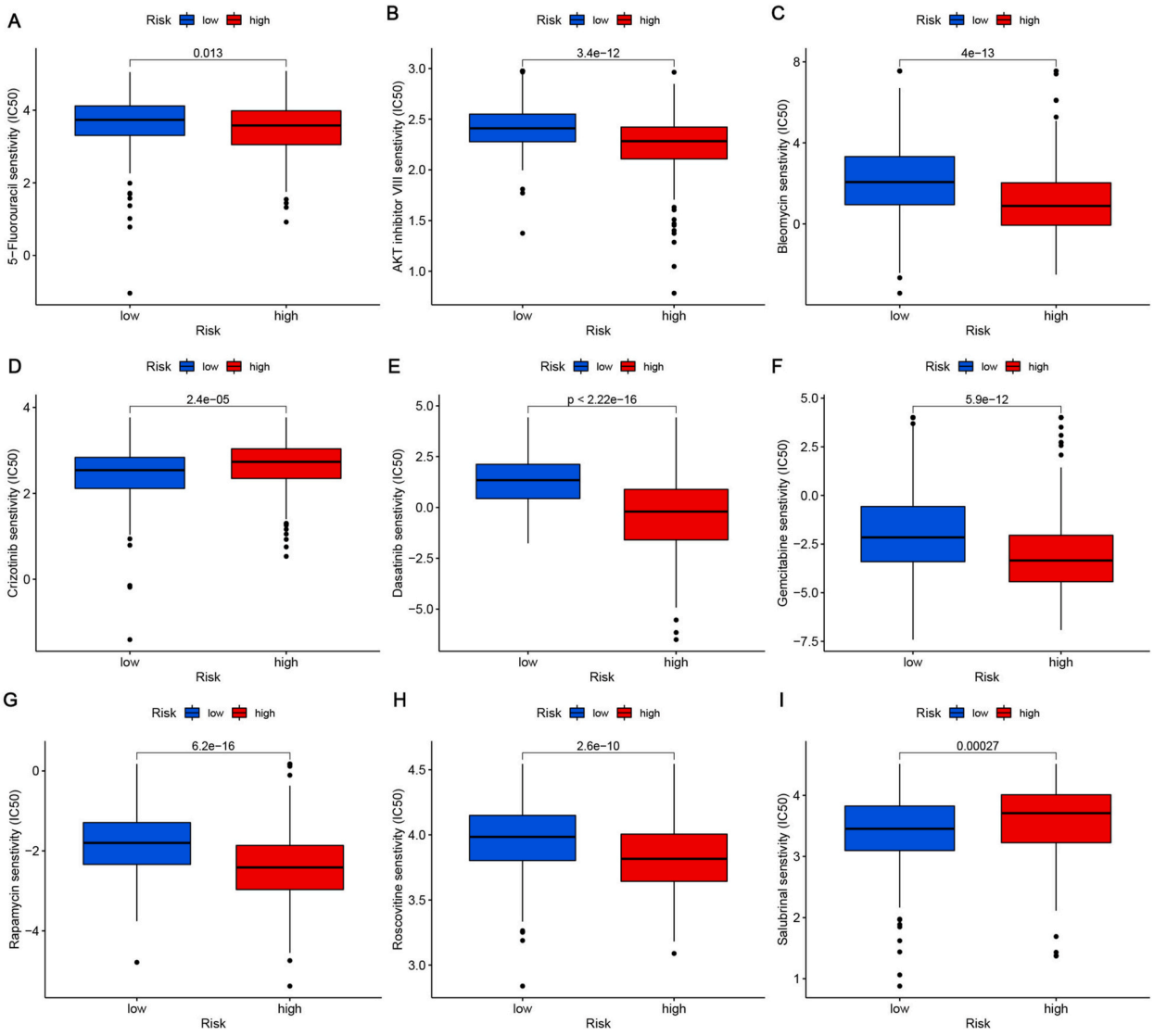

Fig. 10. Therapeutic response analysis of (A) 5-Fluorouracil, (B) AKT inhibitor VIII, (C) Bleomycin, (D) Crizotinib, (E) Dasatinib, (F) Gemcitabine, (G) Rapamycin, (H) Roscovitine, (I) Salubrinal.

macrophages (TAMs); these macrophages are strongly correlated with a poor prognosis in cancer [26]. However, only neutrophil infiltration appeared to be considerably low in the C1 cluster. Substantial evidence indicated that neutrophils have a conspicuous part in cancer progression by releasing factors affecting the TME, thereby directly eliminating cancer cells and producing reactive oxygen and nitrogen species [27]. The dismal prognosis observed in the C1 cluster may be due to the lack of these antitumor effects.

Next, 58 ICGs with prognostic significance were extensively investigated using univariate Cox regression analysis so that a signature could be developed based on these results. The LASSO Cox regression analysis resulted in the selection of 8 genes (PPP2R5C, TNFRSF14, IFNGR2, MAP2K3, MCC, MYD88, NFATC3, and PLCG1) for constructing the prognostic model. The outcomes revealed PPP2R5C to be the only protective factor, whereas the others were risk factors for LGG. PPP2R5C, a regulatory subunit of PP2A, showed an increase or decrease in expression in various tumor types [28–31]. Several studies revealed its close contact with cancer development. One mechanism appeared to inhibit cell proliferation and anchorage-independent growth via dephosphorylation of p53 on Thr55 [32–35]. PPP2R5C was shown to have a positive correlation with the prognosis of LGG patients in this study; nevertheless, further research is needed in this area. The TNF superfamily member TNFRSF14 is responsible for imparting complexity to the potential targets and actions in vivo [36]. Shen et al. reported that PRDM1 is likely to be positively correlated with TNFRSF14 in LGG with an unfavorable prognosis [37]; this was in accord with the negative influence of TNFRSF14 in our model. NFATC3 is a transcription factor of the NFAT family [38], and there are a variety of cellular settings in which it has a function in regulating cell proliferation and differentiation. To illustrate, NFATC3 increased the aggressiveness of angiosarcoma or active tumor development in oral/oropharyngeal squamous cell carcinomas [39–41]. However, other studies have reported that NFATC3 can act as a tumor

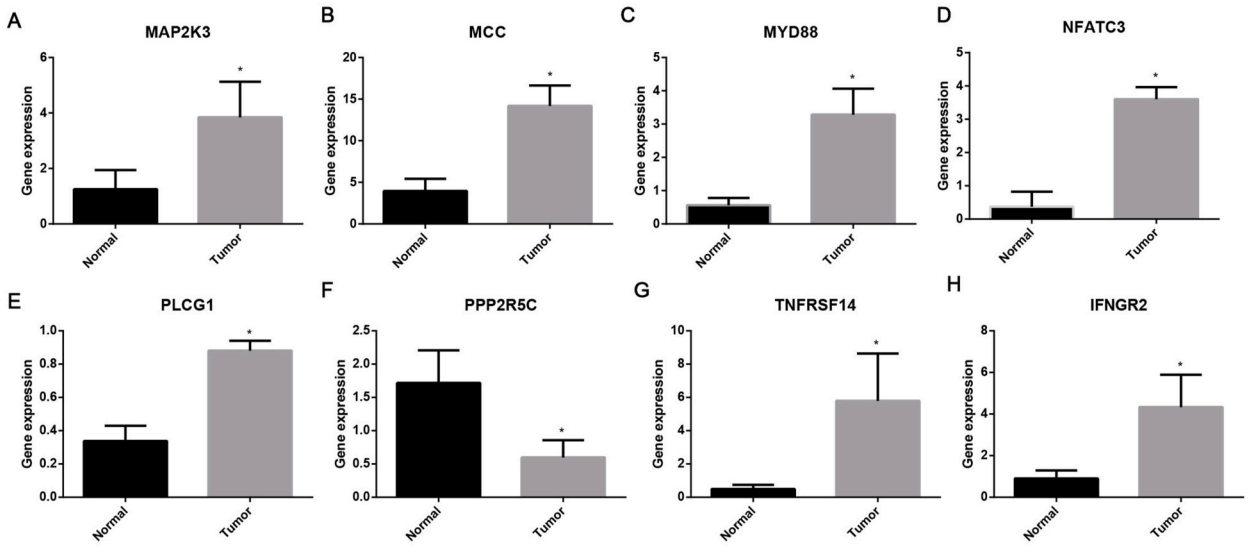

Fig. 11. The expression levels of the eight genes involved in the risk model in tumor cell line U251 and normal cells line HMO6 were detected by RNA-sequencing. (A) MAP2K3. (B) MCC. (C) MYD88. (D) NFATC3. (E) PLCG1. (F) PPP2R5C. (G) TNFRSF14. (H) IFNGR2. *P < 0.05.

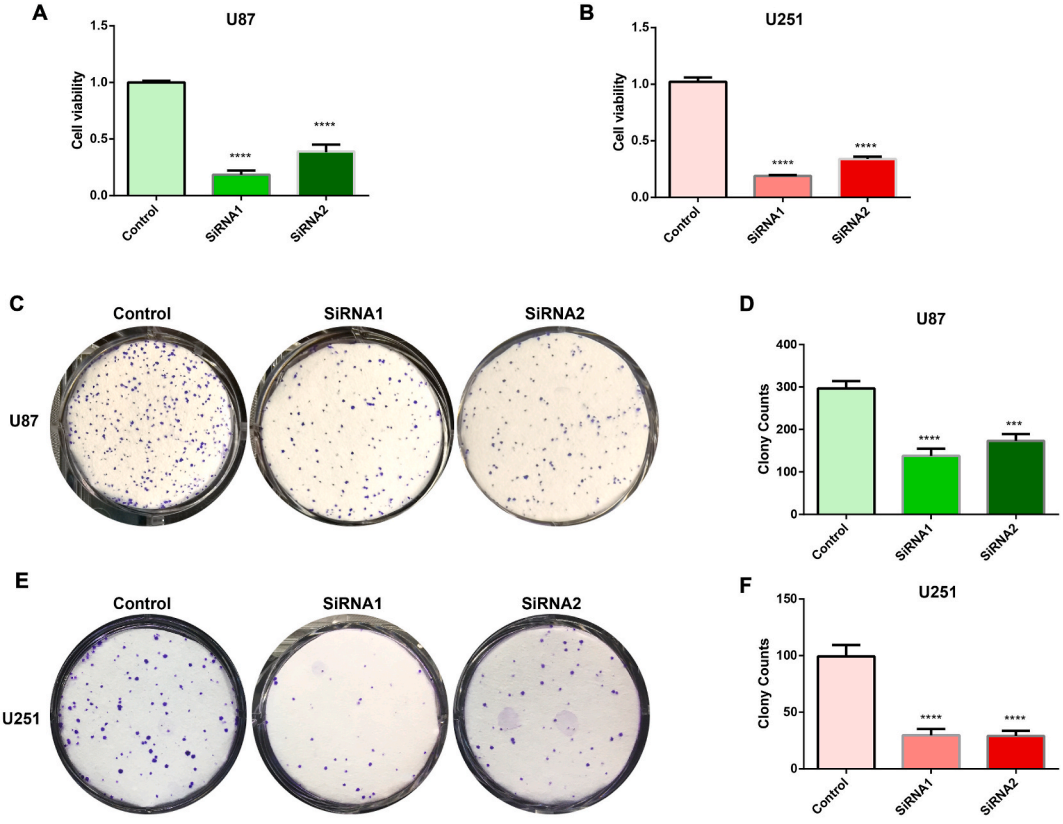

Fig. 12. Knockdown of MCC significantly suppressed proliferation in glioma cells. CCK-8 suggested that knockdown of MCC suppressed the proliferation of U87 (A) and U251 (B) cell lines. (C–D) Knockdown of MCC inhibited colony formation of U87 cells. (E–F) Knockdown of MCC inhibited colony formation of U251 cells. ***P < 0.001, ****P < 0.0001.

suppressor, as observed in cases of T-cell lymphoma and breast cancer [40,42,43]. MYD88 is the canonical adaptor for toll-like receptor and interleukin-1 signaling [44,45], which had been reported to be an adverse prognostic factor in ovarian cancer and a therapeutic target for inflammatory lung diseases [46,47]. However, the role of MYD88 in malignant tumors is largely unknown. Here we proved that PPP2R5C were remarkably downregulated in tumor cell lines while the other seven genes involved in the model were upregulated in tumor cells, which indicated that they were probably excellent biomarkers for prognosis prediction. The clinical role as well as underlying mechanisms of these genes in cancer are needed to explore in future. Based on the median risk score, patients with LGG were categorized into high- and low-risk groups. The high-risk group, in contrast with the low-risk group, has lower survival rates and shorter survival duration, along with low expression levels of PPP2R5C and high expression levels of the other genes.

This research suggested that age, grade, and risk score were all useful prognostic markers, with the risk score standing on its own as a potentially useful prognostic indicator. A nomogram plot involving the abovementioned prognostic predictors was plotted for predicting the survival probability of LGG patients. The satisfied AUC values of the ROC suggested the presence of a remarkable prognostic ability of the nomogram. Given the superior performance of the nomogram, it enables physicians to create a more personalized monitoring plan for LGG, leading to improved outcomes.

Gene alteration is considered a common phenomenon in tumor development. The outcomes of the present study demonstrated that IDH1 and TP53 were the most remarkably altered genes in patients with LGG. IDH1 mutations are rare in cases of cancer in humans; however, they are prevalent in gliomas [48–50]. The initial discovery revealed widespread IDH1 mutations at Arg132 [51,52]. According to the literature, TP53 is an independent predictor of OS in LGG [53]. Notably, the co-occurrence of IDH1 mutation and TP53 alteration indicated a significant tissue-specific role in glioma [54]; thus, this phenomenon may be considered a predictor of patient outcomes in LGG. Furthermore, we assessed the indicative role of prognostic models on TIME. The immune cells within TIME perform a vital function in terms of tumor promotion or tumor antagonization. As anticipated, the high-risk group had higher values than the low-risk group in terms of the ESTIMATE, stroma, and immune scores. Besides, the infiltration level of macrophage M0, macrophage M1, macrophage M2, and resting NK cells were high, whereas eosinophils, monocytes, activated NK cells, and plasma cells were low. Metabolic alterations in macrophages play a predominant role in regulating their suppressive or activating roles in the TIME and may have great potential for immune-responsive cancer treatment [55]. The increased expression of ICGs and high tumor mutational burden are correlated with a poor survival prognosis, demonstrating the fact that these populations are more likely to benefit from treatment with immune checkpoint inhibitors. As for chemotherapy, the present study demonstrated that low-risk groups may benefit from crizotinib and salubrinal whereas high-risk groups had a better response to 5-fluorouracil, AKT inhibitor VIII, bleomycin, dasatinib, gemcitabine, rapamycin, and roscovitine. The aforementioned findings are intended to give some evidence and build the groundwork for future drug development research.

There are some limitations to the current investigation, and additional clinical trials are needed to assess the effectiveness and feasibility of this paradigm. Second, more pathology samples of patients should be included to validate the expression of signature genes, and in vivo or in vitro functional experiments are needed to verify the roles of signature genes. Additionally, fundamental research investigations are required to elucidate the critical function of immune checkpoints and their inhibitors in the LGG process.

Conclusion

The immune checkpoint-related signatures may serve as a novel indicator in the prognosis and immunotherapy response of patients with LGG.

Author contribution statement

Zhixuan Wu; Zhepei Wang; Yangyang Guo: Conceived and designed the experiments; Contributed reagents, materials, analysis tools or data; Wrote the paper. Danfeng Lin; Jingxia Bao: Performed the experiments; Wrote the paper. Kai Hong; Kenan Cen; Jie Sun: Analyzed and interpreted the data; Wrote the paper.

Data availability statement

Data included in article/supplementary material/referenced in article.

Funding

The project was supported by the key research and development program of Ningbo (2022Z125), Ningbo Top Medical and Health Research Program (No.2022020304) and the Ningbo University Institute of Geriatrics (LNBYJS-2021).

Declaration of competing interest

The authors declare that they have no known competing financial interests or personal relationships that could have appeared to influence the work reported in this paper.

Acknowledgements

We thank Bullet Edits Limited for the linguistic editing and proofreading of the manuscript.

Appendix A. Supplementary data

Supplementary data to this article can be found online at https://doi.org/10.1016/j.heliyon.2023.e20178.

References

[1] J.L. Fisher, et al., Epidemiology of brain tumors, Neurol. Clin. 25 (4) (2007) 867–890, vii.
[2] H.L. Smith, N. Wadhwani, C. Horbinski, Major features of the 2021 WHO classification of CNS tumors, Neurotherapeutics 19 (6) (2022) 1691–1704.
[3] T.J.C. Wang, M.P. Mehta, Low-grade glioma radiotherapy treatment and trials, Neurosurg. Clin. 30 (1) (2019) 111–118.
[4] Y. Laviv, et al., BRAF, GNAQ, and GNA11 mutations and copy number in pediatric low-grade glioma, FEBS Open Bio 2 (2012) 129–134.
[5] M.C. Tom, et al., Management for different glioma subtypes: are all low-grade gliomas created equal? Am Soc Clin Oncol Educ Book 39 (2019) 133–145.
[6] A.K. Gnekow, et al., Low grade chiasmatic-hypothalamic glioma-carboplatin and vincristin chemotherapy effectively defers radiotherapy within a comprehensive treatment strategy – report from the multicenter treatment study for children and adolescents with a low grade glioma – HIT-LGG 1996 – of the Society of Pediatric Oncology and Hematology (GPOH), Klin. Pädiatr. 216 (6) (2004) 331–342.
[7] S.C. Wei, C.R. Duffy, J.P. Allison, Fundamental mechanisms of immune checkpoint blockade therapy, Cancer Discov. 8 (9) (2018) 1069–1086.
[8] L. Holokai, et al., Murine- and human-derived autologous organoid/immune cell Co-cultures as pre-clinical models of pancreatic ductal adenocarcinoma, Cancers 12 (12) (2020).
[9] B. Li, H.L. Chan, P. Chen, Immune checkpoint inhibitors: basics and challenges, Curr. Med. Chem. 26 (17) (2019) 3009–3025.
[10] C. Thallinger, et al., Review of cancer treatment with immune checkpoint inhibitors : current concepts, expectations, limitations and pitfalls, Wien Klin. Wochenschr. 130 (3–4) (2018) 85–91.
[11] M. Lim, et al., Current state of immunotherapy for glioblastoma, Nat. Rev. Clin. Oncol. 15 (7) (2018) 422–442.
[12] E.K. Nduom, M. Weller, A.B. Heimberger, Immunosuppressive mechanisms in glioblastoma, Suppl 7, Neuro Oncol. 17 (Suppl 7) (2015). vii9-vii14.
[13] W. Niu, L. Jiang, A seven-gene prognostic model related to immune checkpoint PD-1 revealing overall survival in patients with lung adenocarcinoma, Math. Biosci. Eng. 18 (5) (2021) 6136–6154.
[14] D. Song, et al., A model of seven immune checkpoint-related genes predicting overall survival for head and neck squamous cell carcinoma, Eur. Arch. Oto-Rhino-Laryngol. 278 (9) (2021) 3467–3477.
[15] J.P. Brunet, et al., Metagenes and molecular pattern discovery using matrix factorization, Proc. Natl. Acad. Sci. U.S.A. 101 (12) (2004) 4164–4169.
[16] E. Becht, et al., Estimating the population abundance of tissue-infiltrating immune and stromal cell populations using gene expression, Genome Biol. 17 (1) (2016) 218.
[17] A.M. Newman, et al., Robust enumeration of cell subsets from tissue expression profiles, Nat. Methods 12 (5) (2015) 453–457.
[18] F. Finotello, et al., Molecular and pharmacological modulators of the tumor immune contexture revealed by deconvolution of RNA-seq data, Genome Med. 11 (1) (2019) 34.
[19] T. Li, et al., TIMER2.0 for analysis of tumor-infiltrating immune cells, Nucleic Acids Res. 48 (W1) (2020) W509–w514.
[20] A. Subramanian, et al., Gene set enrichment analysis: a knowledge-based approach for interpreting genome-wide expression profiles, Proc. Natl. Acad. Sci. U.S. A. 102 (43) (2005) 15545–15550.
[21] V. Thorsson, et al., The immune landscape of cancer, Immunity 48 (4) (2018) 812–830.e14.
[22] Q.T. Ostrom, et al., CBTRUS statistical report: primary brain and central nervous system tumors diagnosed in the United States in 2006-2010, Suppl 2, Neuro Oncol. 15 (Suppl 2) (2013). ii1-56.
[23] M. Zhang, et al., Novel immune-related gene signature for risk stratification and prognosis of survival in lower-grade glioma, Front. Genet. 11 (2020) 363.
[24] W. Zou, J.D. Wolchok, L. Chen, PD-L1 (B7-H1) and PD-1 pathway blockade for cancer therapy: mechanisms, response biomarkers, and combinations, Sci. Transl. Med. 8 (328) (2016) 328rv4.
[25] Q. Wu, et al., Small molecule inhibitors targeting the PD-1/PD-L1 signaling pathway, Acta Pharmacol. Sin. 42 (1) (2021) 1–9.
[26] K. Hussain, M.S. Cragg, S.A. Beers, Remodeling the tumor myeloid landscape to enhance antitumor antibody immunotherapies, Cancers 13 (19) (2021).
[27] R.V. Sionov, Leveling up the controversial role of neutrophils in cancer: when the complexity becomes entangled, Cells 10 (9) (2021).
[28] M. Deichmann, et al., The protein phosphatase 2A subunit Bgamma gene is identified to be differentially expressed in malignant melanomas by subtractive suppression hybridization, Melanoma Res. 11 (6) (2001) 577–585.
[29] G. Francia, et al., Identification by differential display of annexin-VI, a gene differentially expressed during melanoma progression, Cancer Res. 56 (17) (1996) 3855–3858.
[30] W. Chen, et al., Identification of specific PP2A complexes involved in human cell transformation, Cancer Cell 5 (2) (2004) 127–136.
[31] H. Zheng, et al., Expression and distribution of PPP2R5C gene in leukemia, J. Hematol. Oncol. 4 (2011) 21.
[32] H.H. Li, et al., A specific PP2A regulatory subunit, B56gamma, mediates DNA damage-induced dephosphorylation of p53 at Thr55, EMBO J. 26 (2) (2007) 402–411.
[33] G.P. Shouse, X. Cai, X. Liu, Serine 15 phosphorylation of p53 directs its interaction with B56gamma and the tumor suppressor activity of B56gamma-specific protein phosphatase 2A, Mol. Cell Biol. 28 (1) (2008) 448–456.
[34] Y. Nobumori, et al., B56γ tumor-associated mutations provide new mechanisms for B56γ-PP2A tumor suppressor activity, Mol. Cancer Res. 11 (9) (2013) 995–1003.
[35] G.P. Shouse, et al., ATM-mediated phosphorylation activates the tumor-suppressive function of B56γ-PP2A, Oncogene 30 (35) (2011) 3755–3765.
[36] C.F. Ware, Targeting lymphocyte activation through the lymphotoxin and LIGHT pathways, Immunol. Rev. 223 (2008) 186–201.
[37] L. Shen, et al., Role of PRDM1 in tumor immunity and drug response: a pan-cancer analysis, Front. Pharmacol. 11 (2020), 593195.
[38] G.R. Crabtree, E.N. Olson, NFAT signaling: choreographing the social lives of cells, Cell 109 (Suppl) (2002) S67–S79.
[39] S.H. Lee, et al., Orai1 promotes tumor progression by enhancing cancer stemness via NFAT signaling in oral/oropharyngeal squamous cell carcinoma, Oncotarget 7 (28) (2016) 43239–43255.
[40] S.H. Lee, et al., NFATc3 plays an oncogenic role in oral/oropharyngeal squamous cell carcinomas by promoting cancer stemness via expression of OCT4, Oncotarget 10 (23) (2019) 2306–2319.
[41] A. Courtwright, et al., Secreted frizzle-related protein 2 stimulates angiogenesis via a calcineurin/NFAT signaling pathway, Cancer Res. 69 (11) (2009) 4621–4628.
[42] S.Z. Glud, et al., A tumor-suppressor function for NFATc3 in T-cell lymphomagenesis by murine leukemia virus, Blood 106 (10) (2005) 3546–3552.
[43] B.K. Robbs, et al., Dual roles for NFAT transcription factor genes as oncogenes and tumor suppressors, Mol. Cell Biol. 28 (23) (2008) 7168–7181.
[44] J. Deguine, G.M. Barton, MyD88: a central player in innate immune signaling, F1000Prime Rep 6 (2014) 97.

[45] A. Lingel, et al., Kaposi's sarcoma-associated herpesvirus reduces cellular myeloid differentiation primary-response gene 88 (MyD88) expression via modulation of its RNA, J. Virol. 90 (1) (2016) 180–188.
[46] F. Di Padova, V.F.J. Quesniaux, B. Ryffel, MyD88 as a therapeutic target for inflammatory lung diseases, Expert Opin. Ther. Targets 22 (5) (2018) 401–408.
[47] C.J. d'Adhemar, et al., The MyD88+ phenotype is an adverse prognostic factor in epithelial ovarian cancer, PLoS One 9 (6) (2014), e100816.
[48] S. Zheng, et al., Prospective clinical sequencing of adult glioma, Mol. Cancer Therapeut. 18 (5) (2019) 991–1000.
[49] H. Yan, et al., IDH1 and IDH2 mutations in gliomas, N. Engl. J. Med. 360 (8) (2009) 765–773.
[50] D. Shen, et al., Landscape of IDH1/2 mutations in Chinese patients with solid tumors: a pan-cancer analysis, Mol Genet Genomic Med 9 (8) (2021) e1697.
[51] D.W. Parsons, et al., An integrated genomic analysis of human glioblastoma multiforme, Science 321 (5897) (2008) 1807–1812.
[52] J. Balss, et al., Analysis of the IDH1 codon 132 mutation in brain tumors, Acta Neuropathol. 116 (6) (2008) 597–602.
[53] C.M.S. Tesileanu, et al., Non-IDH1-R132H IDH1/2 mutations are associated with increased DNA methylation and improved survival in astrocytomas, compared to IDH1-R132H mutations, Acta Neuropathol. 141 (6) (2021) 945–957.
[54] B. Murnyak, L.E. Huang, Association of TP53 alteration with tissue specificity and patient outcome of IDH1-mutant glioma, Cells 10 (8) (2021).
[55] K. Mehla, P.K. Singh, Metabolic regulation of macrophage polarization in cancer, Trends Cancer 5 (12) (2019) 822–834.